Accepted Manuscript

Please cite this article as: Ellie Yi Lih Teo, Lingeswarran Muniandy, Eng-Poh Ng,
Farook Adam, Abdul Rahman Mohamed, Rajan Jose, Kwok Feng Chong, High surface
area activated carbon from rice husk as a high performance supercapacitor electrode,
Electrochimica Acta http://dx.doi.org/10.1016/j.electacta.2016.01.140

This is a PDF file of an unedited manuscript that has been accepted for publication.
As a service to our customers we are providing this early version of the manuscript.
The manuscript will undergo copyediting, typesetting, and review of the resulting proof
before it is published in its final form. Please note that during the production process
errors may be discovered which could affect the content, and all legal disclaimers that
apply to the journal pertain.

High surface area activated carbon from rice husk as a high performance supercapacitor electrode

Ellie Yi Lih Teo[a†], Lingeswarran Muniandy[b†], Eng-Poh Ng[b], Farook Adam[b], Abdul Rahman Mohamed[c], Rajan Jose[a], Kwok Feng Chong[a*] ckfeng@ump.edu.my

[a]Faculty of Industrial Sciences & Technology, Universiti Malaysia Pahang, 26300 Gambang, Kuantan, Malaysia.

[b]School of Chemical Sciences, Universiti Sains Malaysia, 11800 Pulau Pinang, Malaysia.

[c]School of Chemical Engineering, Universiti Sains Malaysia, Engineering Campus, 14300 Nibong Tebal, Pulau Pinang, Malaysia

[*]Corresponding author. Tel.: +609 5492403.

[†]E.Y.L.T and L.M. contributed equally to this work as first authors.

ABSTRACT

In this study, we report on the application of high surface area activated carbon (AC) derived from rice husks as a supercapacitor electrode. The prepared AC was free from Brønsted or Lewis acid sites, thus making the electrical double layer capacitance as the main charge storage mechanism. Three samples of AC with different surface areas were prepared at different activation temperatures and studied electrochemically using cyclic voltammetry, galvanostatic charge-discharge and electrochemical impedance spectroscopy. All AC samples exhibited good electrochemical performance as supercapacitor electrode. The maximum specific capacitance (147 F g^{-1}) was obtained by the AC sample (surface area of 2696 m^2 g^{-1}) which was prepared at an activation temperature of 850 °C. Detailed impedance studies revealed the low resistivity (0.23 Ω) of AC sample and the fast frequency response (0.11 s) of the supercapacitor electrode.

1. INTRODUCTION

The advancement of technology leads to the high demand for high performance energy storage devices which can supply the desired amount of energy when needed. The electrochemical supercapacitor, or better known as supercapacitor, could be the answer in the quest for high performance energy storage device. Supercapacitor is an energy storage device that can deliver high power output (≥ 10 kW kg^{-1}) with long-term cycle life, in addition to its rapid charge-discharge process [1-5]. Over decades of the growing interests towards nanotechnology, various nanomaterials such as high-surface-area carbon nanomaterials, nanosized metal oxides and conducting polymers were reported to be the potential electrode materials for supercapacitor [4, 6-8]. However, the production cost and the industrial applicability limit the large scale production of these nanomaterials as the supercapacitor electrodes.

To date, activated carbon (AC) is the most widely used material for supercapacitor electrode, due to its low cost, high specific surface area and good conductivity [9, 10]. AC is a carbonaceous material which is produced from a wide variety of carbon-rich raw materials such as wood and coal [10-16]. The production of AC typically involves two stages where the raw materials are first carbonized at low temperature, followed by activation at higher temperature [17-19]. Various types of agricultural wastes such as coconut shells, rice husks and empty fruit bunches of oil palm [20-25] were reported as the raw materials for the production of AC in the effort to reduce the production cost and to preserve the environment.

Rice husks (RH) are considered to be an agricultural waste which is found abundantly in rice producing countries. Approximately 122-163 million metric tons of RH are being disposed as waste annually around the world [26]. RH has >37% carbon element by weight [27], thus making it a promising raw material for the production of AC. However, high silica content (more than 20%) [28] in RH must be removed prior to the activation of the AC to ensure that AC with high carbon content is obtained. Our previous work reported on the production of AC with high carbon content (ca. 92% carbon content) and surface area (ca. 2696 m^2/g) through the removal of silica *via* alkali leaching at room temperature (ca. 30 °C) [29]. The prepared AC has low oxygen content and is free from Brønsted or Lewis acid sites, thus rendering it a potential candidate as a supercapacitor electrode with electrical double layer capacitance as the predominant charge storage mechanism. In this work, three different AC samples derived from RH with varying surface areas were activated at various

temperatures. These AC samples were studied electrochemically to evaluate their performances as supercapacitor electrodes which were then compared with other AC samples as reported in the literature.

2.   EXPERIMENTAL

2.1.   Sample preparation

Sodium hydroxide pellets (NaOH, 99%), potassium hydroxide pellets (KOH, 99%) and nitric acid (HNO$_3$, 69%) were obtained from Qrec. Polyvinylidenefluoride (PVDF) and *N*-methyl-2-pyrrolidone (NMP, 99%) were obtained from Sigma-Aldrich. Rice husks (RH) was obtained from a rice mill in Penang, Malaysia. All chemicals were of analytical grade and used without purification.

The detailed experimental procedure for AC preparation was reported in our previous work [29]. Typically, 25 g of rinsed rice husk (RH) was treated with 500 mL of 1 M NaOH solution for 24 h under room condition before being filtered and dried in an oven for another 24 h. The alkali treated RH was later carbonized in a muffle furnace at 400 °C for 4 h to yield the rice husk charcoal (RHC). This RHC was stirred with 300 mL of 1 M NaOH solution at room temperature for 20 min to remove any traces of silica in order to obtain a much purer form of RHC. The RHC was then washed with copious amount of distilled water before being filtered and dried. Activation was carried out by impregnating the RHC with the required amount of KOH (RHC: KOH = 1:5 by mass) before being stirred for 30 min and proceeded by sonication for 15 min. The samples were dried at 100 °C overnight before being activated at various temperatures (750, 850 and 950 °C) for 1 h under nitrogen aeration. The AC samples were then washed until pH 7 with distilled water, filtered and dried for further study. AC obtained from the three activation temperatures were named AC750, AC850 and AC950, respectively, and their surface area and porosity values were listed as in Table 1 [29].

2.2.   Physical characterizations

2.2.1.   Spectroscopy analyses

The functional groups of the AC samples were identified using Fourier transform infrared (FTIR) spectroscopy. Typically, the FTIR spectra were recorded on a Perkin Elmer spectrophotometer (System 2000) using the KBr pellet technique (KBr: sample weight ratio = 150:1). The surface area of the AC samples were determined *via* N_2 adsorption-desorption analysis (Micromeritics ASAP 2020 porosimeter). The AC samples were degassed at 110 °C for 10 h under vacuum prior to the analysis. The surface area of the AC samples were calculated from the BET (Brunauer–Emmett–Teller) equation. The micropore volume was determined through the calculations from the t-plot (Harkins-Jura equation) whereas the mesopore volume was obtained through the BJH (Barret-Joyner Halenda) model for surface analysis. The carbon structures present in the AC sample were determined by Raman spectroscopy (Renishaw inVia Raman microscope), with HeNe laser (633 nm, 2 mW). X-ray photoelectron spectroscopy (XPS) analysis was conducted to investigate the carbon bonds in the AC sample. XPS analysis was acquired using a Kratos photoelectron spectrometer (AXIS Ultra DLD), equipped with an Al Kα x-ray source (1486.6 eV). The analysis was performed *via* hybrid lens mode with the slot aperture; the passing energy of the hemispherical layer was set to 160 eV for the wide survey scan and 20 eV for the narrow scan. Thermal analysis (TGA/SDTA 851^e Mettler Toledo) was carried out to study the stability of the AC sample under oxygenated conditions with a fixed heating rate at 10 °C min^{-1} for temperatures ranging from 30 °C to 920 °C. Total carbon (TC) content in the AC samples was analyzed using Shimadzu SSM-5000A with furnace temperature set at 900 °C.

2.2.2. Microscopy analyses

The surface structures of the AC samples were analyzed using a Leica scanning electron microscope (SEM, Cambridge 360). The topographical features of the samples were investigated using a Philips transmission electron microscope (TEM, CM-12). The AC samples were first added into 15 mL of purified ethanol (99%), and sonicated for 15 min before being placed onto the copper grid for TEM analysis.

2.3.   Electrochemical measurements

AC, carbon black and PVDF were mixed in a mass ratio of 90:5:5. The mixture was stirred overnight to form a homogenous slurry. The slurry was brush-coated onto a nickel foam and dried at 80 °C for 24 h. The brush-coated nickel foam was subsequently punched into

electrodes with diameter of approximately 9 mm. The electrochemical performance of the AC electrodes was characterized with the coin cell configuration with glass microfiber as the separator and 6 M KOH as the electrolyte. The coin cell set up was connected to an Autolab potentiostat/galvanostat (PGSTAT M101) for electrochemical studies. Cyclic voltammetry (CV) and galvanostatic charge-discharge (CDC) were carried out at a potential range of 0–1 V. Electrochemical impedance spectroscopy (EIS) tests were conducted over the frequency range of 500 kHz to 0.01 Hz at an open circuit potential. The electrochemical stability test was performed by repeating the charge/discharge test at current density of 1 A g^{-1} for 10000 cycles.

3.   RESULTS AND DISCUSSION

3.1.   Physical characterizations

The FTIR spectra in Figure 1 indicate that the AC samples consist of several functional groups. Basically, the peaks appearing at 1570-1580 cm^{-1} is attributed to the presence of aromatic C=C bonds [30]. As can be seen, AC850 exhibited the highest peak intensity, thus revealing the presence of the highest amount of C=C aromatic bonds among the samples. In addition, a broad peak in the region of 3400-3500 cm^{-1} could be associated to the O–H stretching from the adsorbed moisture [31]. The sharp peak at 1380 cm^{-1} is due to the traces of nitrate ions (NO_3^-) from the nitric acid which was used to neutralize the KOH (activation agent) of the AC samples [32]. The band at 1096 cm^{-1} is an indicative on the presence of C–O bonds from esters and ethers [31]. As shown, AC850 exhibited the lowest intensity for this band, thus indicating that this sample contains the lowest degree of oxygen content. In contrast, AC950 has the highest degree of oxygen content which can be proven by its highest intensity of C–O band. The findings are consistent with the elemental analysis shown in Table 2.

The carbon structure of AC750, AC850 and AC950 were further investigated by Raman spectroscopy (inset of Figure 1). Two noticeable peaks were observed at 1341 cm^{-1} and 1582 cm^{-1} which correspond to the D and G bands, respectively [33]. The D band (1341 cm^{-1}) is attributed to the turbostratic/disordered carbonaceous structure of the activated carbon [34]. Hence, it is known that the D-band represents the defect sites on the carbonaceous structure of the AC samples. While, the G band (1582 cm^{-1}) is due to the

6

presence of C=C stretching vibrations (sp^2 hybridization) [34] in the AC samples. The R values and crystallite sizes (L_a) in Table 1 were calculated from the following equations:

$$R = \frac{I_D}{I_G} \tag{1}$$

$$L_a(nm) = \frac{4.4}{R} \tag{2}$$

The high I_D/I_G (1.00 ± 0.07) values obtained for all three AC samples indicate high percentage of structural defects in the AC samples which could be related to the activation process by KOH [35].

Table 1 tabulates the textural properties of the AC samples used in the present study. It is observed that the mesopore volume increased from 0.243 cm^3 g^{-1} to 1.056 cm^3 g^{-1} as the activation temperature was raised from 750 °C to 950 °C. However, on the contrary, the micropore volume had dwindled from 0.589 cm^3 g^{-1} to 0.052 cm^3 g^{-1} as the activation temperature was increased from 750 °C to 950 °C under nitrogen aeration. In addition, the micropore area of the AC samples showed a significant decrease from AC750 to AC950. The micropore area for AC750 was found to be 1426 m^2 g^{-1} which decreased to 486 m^{2}g^{-1} for AC850. AC950, however, did not exhibit any micropore area as shown in Table 1. These observations could explain the instability of the micropores upon thermal activation. The raising of the activation temperature would in fact lead to the collapse of the microporous structures in the AC samples. The collapse of these micropores would consequently pave the way for the formation of the mesoporous structures in the AC samples as proven in Table 1. However, the destruction of micropores would result in lower surface area as can be seen in AC950 (1592 m^{2}g^{-1}) in comparison to AC750 (2121 m^{2}g^{-1}) and AC850 (2696 m^{2}g^{-1}). Scheme 1 clearly illustrates the collapse of smaller pores in AC750 forming larger meso/macropores upon higher activation temperature such as in AC950. The same observations were also reported by Kong et al. [36].

Figure 2a shows the XPS spectrum generated from AC850, with both carbon and oxygen elements as its main moiety. Figure 2b shows the narrow scan for the C 1s electron orbital and it was found that the main peak at 284.6 eV is attributed to the presence of conjugated C=C sp^2 hybridized bonds [37]. Furthermore, a recent paper by Singh *et al.*

claimed that the peak in the range of 284-285.5 eV is mainly attributed to the presence of C=C aromatic bond (C 1s-$\pi^{*}_{C=C}$) [38, 39]. A secondary peak at 286 eV was obtained and it suggests the presence of the C–C sp^3 hybridized bonds [37] and C-O groups [40]. Another satellite peak was also observed at 288.1 eV which could be due to the presence of carbonyl (C=O), carboxylic (COOH) groups [38]. The other two peaks at 293 eV and 295.7 eV could be related to the formation of sodium carbonate and potassium carbonate, respectively [39].

The deconvolution of the O 1s band exhibited several peaks with various binding energies, as shown in Figure 2c. The peak appearing at 534.0 eV (89.6%) indicates the presence of ether linkages/bonds (C-O-C) and also is attributed due to the chemisorbed moisture onto the surface of the AC sample forming the C-OH bonds [40, 41]. A second peak was observed at ~530.8 eV (9.2%) which is attributed to the presence of carbonyl groups (C=O) originating from a ketone/aldehyde [41].

The SEM images in Figures 3a, c and e reveal that all the AC samples were filled with hollow tunnels which could be attributed to the gasification of volatiles upon activation [42]. All of the AC samples consist of very fine particles in agglomeration, as shown from TEM images (Figures 3b, d and f). In addition, it could be clearly seen that the carbon particles were disordered/turbostratic in all AC samples, hence are in agreement with the Raman analyses. The elemental analysis carried out on the three AC samples (Table 2) have shown that AC750 and AC850 consist predominantly of carbon based materials with very low oxygen content (< 15 wt.%). However, AC950 on the other hand, has far lower carbon content but higher amount of oxygen compared to the other two AC samples. This trend was also observed by Chang et al. [43] in which the authors explained that the decreasing amount of carbon content upon increasing the activation temperature is the result of an increase in gasification reactions as the activation temperature/time increases.

Figure 4 exhibits the TGA-DTG plot for AC850 under oxygenated environment. The TGA-DTG analysis was carried out to study the thermal stability of the AC sample under oxygenated conditions with a steady heating rate of 10 °C min^{-1}. It was observed that the weight loss of the AC sample was gradual and happened under several stages of temperature. The first stage of weight loss occurred between 30–166 °C. This weight loss amount to 32.45 wt.% which was attributed to the evaporation of the moisture content which was initially adsorbed onto the surface of the AC [44]. Furthermore, the weight loss at this stage was also contributed to the loosely held organic volatiles which burnt rapidly under the oxygenated

atmosphere [45]. As the heating prolonged to 16–6–358 °C, the second stage of weight loss occurred amounting to 16.76 wt.%. This was due to the burning of the cellulose and hemi-cellulose materials [40]. The final stage of weight loss took place from 357 to 920 °C in which about 37.60 wt.% loss was observed probably due to the decomposition of lignin [45]. This eventually resulted with only 13.20 wt.% of the AC residue left after the combustion process. This could have been the result of the formation of heat resistant graphitic/carbide particles upon reaction with the oxygenated atmosphere hence, would require higher heating temperature and duration.

3.2. Electrochemical studies

Figure 5a shows the CV curves of AC samples at a scan rate of 40 mV s^{-1}. It was observed that the AC750, AC850 and AC950 exhibited quasi-rectangular shape for CV curves, a typical behaviour for electrical double layer capacitance [2, 46]. It also indicates the good charge propagation within the structure in AC750, AC850 and AC950. Besides, no significant redox signal was observed for all CV curves which indicates the absence of pseudo-capacitance in the prepared AC samples and signifies the predominant charge storage mechanism in the prepared AC samples to be electrochemical double layer capacitance. The absence of pseudo-capacitance in AC could be attributed to the insignificant oxygen functional groups within the structure as they could contribute to the faradaic reactions [1, 47]. Such findings are supported by our spectroscopy analyses where the AC consists of mainly C=C aromatic bonds with low oxygen content (Figures 1 and 2). The specific capacitance values of AC were calculated from CV curves by integrating the area under the curve for the average value and they are summarized in Figure 5b. The highest specific capacitance values for AC750, AC850 and AC950 were computed as 127, 143 and 79 F g^{-1}, respectively at 5 mV s^{-1}. The higher specific capacitance values of AC750 and AC850 could be related to the higher surface area (2121 m^2 g^{-1} for AC750; 2696 m^2 g^{-1} for AC850), which led to the higher ions adsorption for double layer capacitance, in comparison to AC950 with lower surface area (1592 m^2 g^{-1}). Furthermore, the highest porosity of the AC850 could contribute to the highest specific capacitance among all three AC samples. AC850 has higher volume of mesopores (0.691 cm^3 g^{-1}) as compared to AC750 (0.243 cm^3 g^{-1}). This enables the electrolyte ions to penetrate as mesopores functions as an electrolyte transport channel to access the micropores adsorption sites for double layer formation. Although AC950 possesses

the highest mesoporous volume among all three AC samples, its micropores volume is very low which results less effective in double layer formation. For all AC samples, it was clearly seen that the specific capacitance values decreased with the increase of scan rate. The increase in scan rate limited the ions accessibility to the electrode surface, therefore making the internal pores inaccessible to the electrolyte ions. However, as the scan rate increased to 100 mV s^{-1}, AC950 suffered significant capacitance drop to 65 F g^{-1}, which is ca. 22% of the value measured at 5 mV s^{-1}. This phenomenon could be related to the ion sieving effect where the ultrafine pores in AC950 could only be accessed at slow diffusion rate [48].

Galvanostatic CDC tests were conducted at various current densities to assess the feasibility of the prepared AC as supercapacitor electrodes. The representative CDC curves of AC750, AC850 and AC950 are displayed in Figure 6a. All three AC samples exhibited insignificant *iR* drop, an indicative of good conductivity. In addition, the AC samples were also displayed symmetrical charging and discharging curves that implies the good reversibility of the electrodes. The bending of the charging curve for all AC samples at high voltage could be attributed to the ionic transport problem at the elevated potential. The specific capacitance values were derived from the slope of the discharging curves and they are summarized in Figure 6b. The highest specific capacitance values were obtained as 123, 147 and 80 F g^{-1} for AC750, AC850 and AC950, respectively at 0.1 A g^{-1}. This is in agreement with the CV findings (Figure 5a). Among three AC samples prepared, AC850 exhibited the best Coulombic efficiency of 96%. The loss of the charge could be due to the cell resistance. The specific capacitance values derived from CDC were used for the energy density and power density calculations, as shown in the following equations:

$$E = \frac{1}{2}CV^2 \tag{3}$$

$$P = \frac{E}{t} \tag{4}$$

where E is the energy density, P is the power density, C is the specific capacitance value, t is the discharging time and V is the potential window. The Ragone plot (Figure 7) reveals the favorable energy rating for AC850 in which the maximum energy density of 5.11 W h kg^{-1} was obtained. It is comparable to other biomass-derived AC such as bamboo (2.0 W h kg^{-1}) [24] and lignin (5.8 W h kg^{-1}) [25]. The electrochemical performance of AC samples in this work and AC samples derived from various biomass precursors are compared in Table 3.

Electrochemical impedance spectroscopy (EIS) was performed to investigate the charge kinetic properties of the prepared AC towards the capacitive behavior. Figure 8 shows the Nyquist plots of AC samples at open circuit potential. The intersection of the *x*-axis is known as the equivalent series resistance (ESR), which incorporates the bulk resistance of the porous carbon material, the bulk resistance of the electrolyte and the contact resistance between the electrode and the current collector. The ESR values were found to be ca. 0.19, 0.23 and 0.30 Ω for AC750, AC850 and AC950, respectively. The charge transfer resistance values (R_{CT}) were obtained by extrapolating the semicircle of the Nyquist plots at high frequency region (inset of Figure 8) and they were measured to be ca. 0.55, 0.27 and 1.33 Ω for AC750, AC850 and AC950, respectively. The low values of ESR and R_{CT} for AC850 could be associated to the optimum activation temperature for AC850 that produced higher amount of C=C bonds, as shown in the FTIR and Raman spectroscopy studies (Figure 1). The higher amount of C=C bonds could facilitate the electron mobility that contributes to lower resistivity in AC850. The almost-vertical line at low frequency region is related to the ions diffusion within the electrode, or better known as Warburg impedance. It can be clearly seen that the Warburg impedance increased in the order of AC850 (2696 m^2/g) < AC750 (2121 m^2/g) < AC950 (1592 m^2/g). This phenomenon could be explained by the high porosity and high surface area of AC850 that enabled smooth diffusion within the AC structure.

The rate capability of the samples was studied using the complex Bode plots, according to the following equations:

$$C'(\omega) = \frac{-Z''(\omega)}{\omega \, |Z(\omega)|^2} \tag{5}$$

$$C''(\omega) = \frac{-Z'(\omega)}{\omega \, |Z(\omega)|^2} \tag{6}$$

where C' represents the real part of the cell capacitance and C'' is the imaginary part related to the losses in the charge storage process leading to an energy dissipation [48]. $Z'(\omega)$ and $Z''(\omega)$ are the respective real and imaginary parts of the complex impedance. ω is the angular frequency and it is given by $\omega = 2\pi f$. Figure 9a shows the variation of C' with the frequency and it shows that the highest capacitance values were attained at low frequency for all samples, with the following order: AC850 > AC750 > AC950. This is in agreement with the CV and CDC findings (Figures 5 and 6). Meanwhile, Figure 9b presents the change of C'' along with the frequency and it was used to deduce the relaxation time constant ($\tau_0 = 1/f_0$), where f_0 is the peak frequency of the imaginary plot [58]. It can be defined as the minimum

time needed to discharge all of the energy with an efficiency of greater than 50% and it also shows the limit between the resistive and the capacitive behaviors of the supercapacitor system [64]. The τ_0 values were computed as 0.22, 0.11 and 0.41 s for AC750, AC850 and AC950 respectively. Again, it shows that the optimum-activation-temperature-produced AC850 had rapid charge storage and delivery. The τ_0 obtained on AC850 shows superiority as compared to those obtained from other reported biomass-derived AC, such as tamarind fruit shell (6.45 s) [65], *Enteromorpha prolifera* (0.86 s) [66], ramie fibers (0.92 s) [67] and hardwood lignin (1.25 s) [24].

Finally, the stability of the samples was tested to evaluate their practical application under long cycle usage. For this purpose, the AC850 with the best electrochemical performance was charged-discharged for 10000 cycles at current density of 1 A g^{-1} (Figure 10). It could be seen that AC850 was found to retain approximately 85% of its capacitance after 10,000 cycles of CDC. The gradual decay of the capacitance could be due to the blocking of the AC micropores at continuous cycling. Such pores blockage could lead to the lower ions adsorption and eventually reduced the specific capacitance. In addition, the CDC curves remained unchanged and the Columbic efficiency was retained at 90% after 10000 cycles. The findings indicate that the RH-derived AC could be the electrode material for deployable supercapacitor with high stability.

4. CONCLUSIONS

In this study, high surface area AC samples, which were derived from rice husk (RH) and activated at different temperatures were studied electrochemically to evaluate their performance as a supercapacitor electrode. The optimum-activation-temperature-produced AC850, which possessed the highest specific surface area and porosity, contributed to good electrochemical performance as supercapacitor electrode. The AC850 was shown to deliver a specific capacitance of 147 F g^{-1} and an energy density of 5.11 W h kg^{-1} in 6 M KOH electrolyte. In addition, AC850 exhibited low resistivity that could be associated with the predominant C=C bonds and low oxygen content in the structure. The electrochemical findings suggest that RH-derived AC is a potentially suitable material for supercapacitor electrode.

ACKNOWLEDGEMENT

13

REFERENCES

[1]   B.E. Conway, Electrochemical Supercapacitors: Scientific fundamentals and technological applications, Kluwer-Plenum, New York, 1999.

[2]   P. Simon, Y. Gogotsi, Materials for electrochemical capacitors, Nature Materials 7 (2008) 845.

[3]   S. Zhang, N. Pan, Supercapacitors performance evaluation, Advanced Energy Materials, 5 (2015) 1401401.

[4]   F. Beguin, V. Presser, A. Balducci, E. Frackowiak, Carbons and electrolytes for advanced supercapacitors, Advanced Materials, 26 (2014) 2219.

[5]   P. Simon, Y. Gogotsi, B. Dunn, Where do batteries end and supercapacitors begin? Science, 343 (2014) 1210.

[6]   Z. Zheng, H. Zhou, X. Long, E. Guo, X. Wang, Electrodeposition of hierarchical manganese oxide on metal nanoparticles decorated nanoporous gold with enhanced supercapacitor performance, Journal of Alloys and Compounds 632 (2015) 376.

[7]   C. Xia, W. Chen, X. Wang, M.N. Hedhili, N. Wei, H.N. Alshareef, Highly stable supercapacitors with conducting polymer core-shell electrodes for energy storage applications, Advanced Energy Materials 5 (2015) 1401805.

[8]   N. Kurra, R. Wang, H.N. Alshareef, All conducting polymer electrodes for asymmetric solid-state supercapacitors, Journal of Materials Chemistry A 3 (2015) 7368.

[9]   G.P. Pandey, A.C. Rastogi, C.R. Westgate, All-solid-state supercapacitors with poly(3,4-ethylenedioxythiophene) coated carbon fiber paper electrodes and ionic liquid gel polymer electrolyte, Journal of Power Sources 245 (2014) 857.

[10]   J. Jiang, L. Zhang, X. Wang, N. Holm, K. Rajagopala, F. Chen, S. Ma, Highly ordered macroporous woody biochar with ultra-high carbon content as supercapacitor electrodes, Electrochimica Acta 113 (2013) 481.

[11]   Z. Jin, X. Yan, Y. Yu, G. Zhao, Sustainable activated carbon fibers from liquefied wood with controllable porosity for high-performance supercapacitors, Journal of Material Chemistry A 2 (2014) 11706.

[12]   Y. Zhou, B. Han, High surface area activated carbon from Chinese coal, Energy & Fuels 15 (2001) 1383.

[13]   Y. Zhang, H. Cui, R. Ozao, Y. Cao, B.I.T. Chen, C. Wang, W. Pan, Characterization of Activated Carbon Prepared from chicken waste and coal, Energy & Fuels 21 (2007) 3735.

[14]   V. Fierro, V. Torne-Fernandez, A. Celzard, Highly microporous carbons prepared by activation of kraft lignin with KOH, Studies in Surface Science and Catalysis 160 (2007) 607.

[15]   V. Fierro, V. Torne-Fernandez, A. Celzard, Methodical study of the chemical of kradt lignin with KOH and NaOH, Microporous and Mesoporous Materials 101 (2007) 419.

[16]   W. Zhao, V. Fierro, N. Fernandez-Huerta, M. T. Izqujerdo, A. Celzard, Impact of synthesis conditions of KOH activated carbons on their hydrogen storage capacities, International Journal of Hydrogen Energy 37 (2012) 14278.

[17]   A. H. Basta, V. Fierro, H. El-Saied, A. Celzard, 2-Steps KOH activation of rice straw: An efficient method for preparing high-performance activated carbons, Bioresource Technology 100 (2009) 3941.

[18]   S. Timur, I.C. Kantarli, E. Ikizoglu, J. Yanik, Preparation of activated carbons from Oreganum stalks by chemical activation, Energy & Fuels 20 (2006) 2636.

[19]   I. Okman, S. Karagoz, T. Tay, M. Erdem, Activated carbons from grape seeds by chemical activation with potassium carbonate and potassium hydroxide, Applied Surface Science 293 (2014) 138.

[20]   T.D. Nguyen, J.K. Ryu, N. B. Sachin, T.N. Kim, Performance of electric double layers capacitor using activated carbon materials from rice husk as electrodes, Korean Journal of Materials Research 23 (2013) 643.

[21]   K. Kuratani, K. Okuno, T. Iwaki, M. Kato, N. Takeichi, T. Miyuki, T. Awazu, M. Majima, T. Sakai, Converting rice husk activated carbon into active material for capacitor using three-dimensional porous current collector, Journal Power Sources 196 (2011) 10788.

[22]   Y. Guo, J. Qi, Y. Jiang, S. Yang, Z. Wang, H. Xu, Performance of electrical double layer capacitors with porous carbons derived from rice husk, Materials Chemistry and Physics 80 (2003) 704.

[23]   K.L. Van, T.T.L. Thi, Activated carbon derived from rice husk by NaOH activation and application in supercapacitor, Progress in Natural Science: Materials International 24 (2014) 191.

[24]   D. Saha, Y. Li, Z. Bi, J. Chen, J.K. Keum, D.K. Hensley, H.A. Grappe, H.M. Meyer, S. Dai, M.P. Paranthaman, A.K. Naskar, Studies on supercapacitor electrode material from activated lignin-derived mesoporous carbon, Langmuir 30 (2014) 900.

[25]   C.S. Yang, Y.S. Jang, H.K. Jeong, Bamboo-based activated carbon for supercapacitor applications, Current Applied Physics 14 (2014) 1616.

[26]   E.-P. Ng, H. Awala, K.-H. Tan, F. Adam, R. Retoux, S. Mintova, EMT-type zeolite nanocrystals synthesized from rice husk, Microporous and Mesoporous Materials 204 (2015) 204.

[27]   A. Salanti, L. Zoia, M. Orlandi, F. Zanini, G. Elegir, Structural characterization and antioxidant activity evaluation of lignins from rice husk, Journal of Agricultural and Food Chemistry 58 (2010) 10049.

[28]   F. Adam, J.-T. Wong, E.-P. Ng, Fast catalytic oxidation of phenol over iron modified zeolite L nanocrystals, Chemical Engineering Journal 214 (2013) 63.

[29]   L. Muniandy, F. Adam, A.R. Mohamed, E.P. Ng, The synthesis and characterization of high purity mixed microporous/mesoporous activated carbon from rice husk using chemical activation with NaOH and KOH, Microporous and Mesoporous Materials 197 (2014) 316.

[30]   C. Saka, BET, TG–DTG, FT-IR, SEM, iodine number analysis and preparation of activated carbon from acorn shell by chemical activation with $ZnCl_2$, Journal of Analytical and Applied Pyrolysis 95 (2012) 21.

[31]   E.-P. Ng, S. Mintova, Quantitative moisture measurements in lubricating oils by FTIR spectroscopy combined with solvent extraction approach, Microchemical Journal 98 (2011) 177.

[32] F. Adam, J.-H. Chua, The adsorption of palmytic acid on rice husk ash chemically modified with Al(III) ion using the sol–gel technique, Journal of Colloid and Interface Science 280 (2004) 55.

[33] H. Jin, X. Wang, Z. Gu, J. D. Hoefelmeyer, K. Muthukumarappan, J. Julson, Graphitized activated carbon based on big bluestem as an electrode for supercapacitors, RSC Advances, 4 (2014) 14136.

[34] T. -X. Shang, R. -Q. Ren, Y. -M. Zhu, X. -J. Jin, Oxygen- and nitrogen-co-doped activated carbon from waste particleboard for potential application in high-performance capacitance, Electrochimica Acta 163 (2015) 32.

[35] I. I. G. Inal, S. M. Holmes, A. Banfordb, Z. Aktas, The performance of supercapacitor electrodes developed from chemically activated carbon produced from waste tea, Applied Surface Science, 357 (2015) 696-703.

[36] J. -J. Kong, Q. -Y. Yue, P. Zhao, B. -Y. Gao, Q. Li, Y. Wang, H. H. Ngo, W. -S. Guo, Comparative study on microstructure and surface properties of keratin and lignocellulosic-based activated carbons, Fuel Processing Technology, 140 (2015) 67-75.

[37] W.M. Silva, H. Ribeiro, L.M. Seara, H.D.R. Callado, A.S. Ferlauto, R.M. Paniago, C.F. Leite, G.G. Silva. Surface properties of oxidized and aminated multiwalled carbon nanotubes, Journal of Brazillian Chemical Society 23 (2012) 1078.

[38] B. Singh, Y. Fang, B.C.C. Cowie, L. Thomsen, NEXAFS and XPS characterisation of carbon functional groups of fresh and aged biochar, Organic Geochemistry 77 (2014) 1.

[39] S. Oswald, Binding energy referencing for XPS in alkali-metal based battery materials research (I): Basic model investigation, Applied Surface Science 351 (2015) 492.

[40] B. Strzemiecka, A. Voelkel, J. D.-Robles, J. M. M.-Martínez, Assessment of the surface chemistry of carbon blacks by TGA-MS, XPS and inverse gas chromatography using statistical chemometric analysis, Applied Surface Science 316 (2014) 315.

[41]   S. Reiche, R. Blume, X. C. Zhao, D. Su, E. Kunkes, M. Behrens, R. Schlogl, Reactivity of mesoporous carbon against water – An in-situ XPS study, Carbon 77 (2014) 175.

[42]   M.A. Lillo-Rodenas, D. Cazorla-Amoros, A. Linares-Solano, Understanding chemical reactions between carbons and NaOH and KOH: An insight into the chemical activation mechanism, Carbon 41 (2003) 267.

[43]   Y.-M. Chang, W.-T. Sai, M.-H. Li, Characterization of activated carbon prepared from chlorella-based algal residue, Bioresource Technology 184 (2015) 344.

[44]   M. Danish, R. Hashim, M. N. M. Ibrahim, O. Sulaiman, Optimized preparation for large surface area activated carbon from date (Phoenix dactylifera L.) stone biomass, Biomass and Bioenergy 61 (2014) 167.

[45]   S. Somasundaram, K. Sekar, V.K. Gupta, S. Ganesan, Synthesis and characterization of mesoporous activated carbon from rice husk for adsorption of glycine from alcohol-aqueous mixture, Journal of Molecular Liquid 177 (2013) 416.

[46]   M.D. Stoller, S. Park, Y. Zhu, J. An, R.S. Ruoff, Graphene-based ultracapacitors, Nano Letters 8 (2008) 3498.

[47]   E. Frackowiak and F. Beguin, Materials for electrochemical storage of energy in capacitors, Carbon 39 (2001) 937.

[48]   E.Y.L. Teo, H.N. Lim, R. Jose, K.F. Chong, Aminopyrene functionalized reduced graphene oxide as a supercapacitor electrode, RSC Advances 5 (2015) 38111.

[49]   V. Subramaniam, C. Luo, A.M. Stephan, K.S. Nahm, S. Thomas, B. Wei, Supercapacitors from activated carbon derived from banana fibers, Journal of the Physical Chemistry C 111 (2007) 7527.

[50]   K.C. Wu, R.L. Tseng, C.C. Hu, C.C. Wang, Effects of pore structure and electrolyte on the capacitive characteristics of steam and KOH-activated carbons for supercapacitors, Journal of Power Sources 144 (2005) 302.

[51]   R. Farma, M. Deraman, A. Awitdrus, I.A. Talib, E. Taer, N.H. Basri, J.G. Marijunatha, M.M. Ishak, B.N.M. Dollah, S.A. Hashmi, Preparation of highly porous binderlesss activated carbon electrodes from fibers of empty fruit brunches for application in supercapacitors, Bioresource Technology 132 (2013) 254.

[52]   E. Taer, M. Deraman, I.A. Talib, Awildrus, S.A. Hashmi, A.A. Umar, Preparation of highly porous binderless activated carbon monolith from rubber wood sawdust buy a multi-step activateion process for application in supercapacitors, International Journal of Electrochemical Science 6 (2011) 3301.

[53]   I.I. Misnon, N.K. Mohd Zain, R. Abdul Aziz, B. Vidyaharan, R. Jose, Electrochemical properties of carbon from oil palm kernel shell for high performance supercapacitors, Electrochimica Acta 174 (2015) 78.

[54]   M. Chen, X. Kang, T. Wumaier, H. Dou, B. Gao, Y. Han, G. Xu, Z. Liu, L. Zhang, Preparation of activated carbon from cotton stalk and its application in supercapacitor, Journal of Solid State Electrochemistry 17 (2013) 1005.

[55]   T. Adinaveen, L. John Kennedy, J. Judith Vijaya, G. Sekaran, Surface and porous characterization of activated carbon prepared from pyrolysis (rice straw) by two-stage procedure and its applications in supercapacitor electrodes, Journal of Material Cycles and Waste Management 17 (2014) 736.

[56]   A. Ganesan K. Mukerjee, J. Raj, M.M. Shaijumon, Nanoporous rice husk derived carbon for gas storage and high performance electrochemical energy storage, Journal of Porous Material 21 (2014), 839.

[57]   S.G. Lee, K.H. Park, W.G. Shim, M.S. Balathanigaimani, H. Moon, Performance of electrochemical double layer capacitors using highly porous activated carbons prepared from beer lees, Journal of Industrial and Engineering Chemistry 17 (2011) 450.

[58]   R.A. Aziz, I.I. Misnon, K.F. Chong, M.M. Yusoff, R. Jose, Layered sodium titanate nanostructures as a new electrode for high energy density supercapacitor, Electrochimica Acta 113 (2013) 141.

[59]   E. Raymundo-Pinero, M. Cadek, F. Beguin, Tuning carbon materials for supercapacitor by direct pyrolysis of seaweeds, Advanced Functional Materials 19 (2009) 1032.

[60]   L. Wei, M. Sevilla, A.B. Fuertes, R. Mokaya, G. Yushin, Hydrothermal carbonization of abundant renewable natural organic chemicals for high-performance supercapacitor electrodes, Advanced Energy Materials 1 (2011) 356-361.

[61]   P. Zhao, Y. Han, X. Dong, C. Zhang, S. Liu, Application of activated carbon derived from scrap tires as electrode materials for supercapacitors, ECS Journal of Solid State Science and Technology 4 (2015) 35.

[62]   L. Chen, T. Ji, L. Brisbin, J. Zhu, Hierachical porous and high surface area tubular carbon as dye adsorbent and capacitor electrode, ACS Applied Materials and Interfaces 7 (2015) 12230.

[63]   D. Kalpana, S.H. Cho, S.B. Lee, Y.S. Lee, R. Misra, N.G. Renganathan, Recycled waste paper-A new source of raw material for electric double-layer capacitors, Journal of Power Sources 2 (2009) 587.

[64]   C. Portet, P.L. Taberna, P. Simon, E. Flahaut, C. Laberty-Robert, High power density electrodes for carbon supercapacitor applications, Electrochemica Acta 50 (2005) 4174.

[65]   S.T. Senthilkumar, R. Kalai Selvan, J.S. Melo, C. Sanjeeviraja, High performance solid-state electric double layer capacitor from redox mediated gel polymer electrolyte and renewable tamarind fruit shell derived porous carbon, ACS Applied Materials and Interfaces 5 (2013) 10541.

[66]   X. Gao, W. Xing, J. Zhou, G. Wang, S. Zhuo, Z. Liu, Q. Xue, Z. Yan, Superior capacitive performance of active carbons derived from *Enteromorpha prolifera*, Electrochimica Acta 133 (2014) 459.

[67]   X. Du, W. Zhao, Y. Wang, C. Wang, M. Chen, T. Qi, C. Hua, M. Ma, Preparation of activated carbon hollow fibers from ramie at low temperature for electric double-layer capacitor applications, Bioresource Technology 149 (2013) 31.

Figure Captions

Figure 1 FTIR and (inset) Raman spectra of the AC samples.

Figure 2 (a) XPS general scan spectrum with (b) C 1s and (c) O 1s narrow scan spectra of AC850.

Figure 3 SEM and TEM images of (a,b) AC750, (c,d) AC850 and (e,f) AC950.

Figure 4 TGA-DTG thermogram of AC850 under oxygenated conditions.

Figure 5 (a) Cyclic voltammogram curves of AC750, AC850 and AC950 at a scan rate of 40 mV s^{-1}, and (b) Plot of specific capacitance of AC750, AC850 and AC950 as a function of scan rate.

Figure 6 (a) Charge discharge curves of AC750, AC850 and AC950 at current density of 0.1 A g^{-1}, and (b) Plot of specific capacitance of AC750, AC850 and AC950 as a function of current density.

Figure 7 Ragone plot for AC750, AC850 and AC950.

Figure 8 Nyquist plot of AC750, AC850 and AC950.

Figure 9 Evolution of (a) real and (b) imaginary part of capacitance versus frequency.

Figure 10 Stability test for AC850 at 1 A g^{-1} for 10000 cycles.
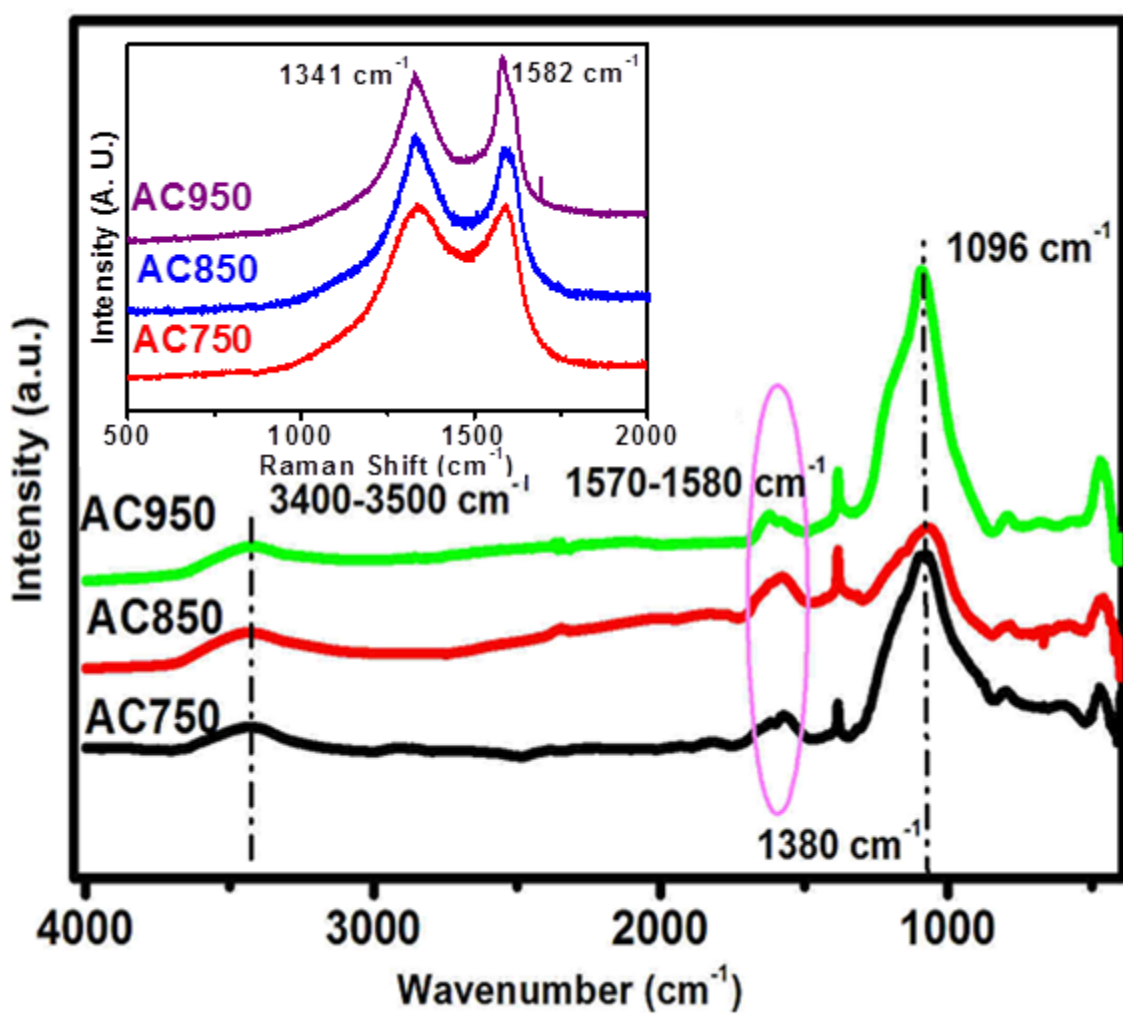
Figure 1
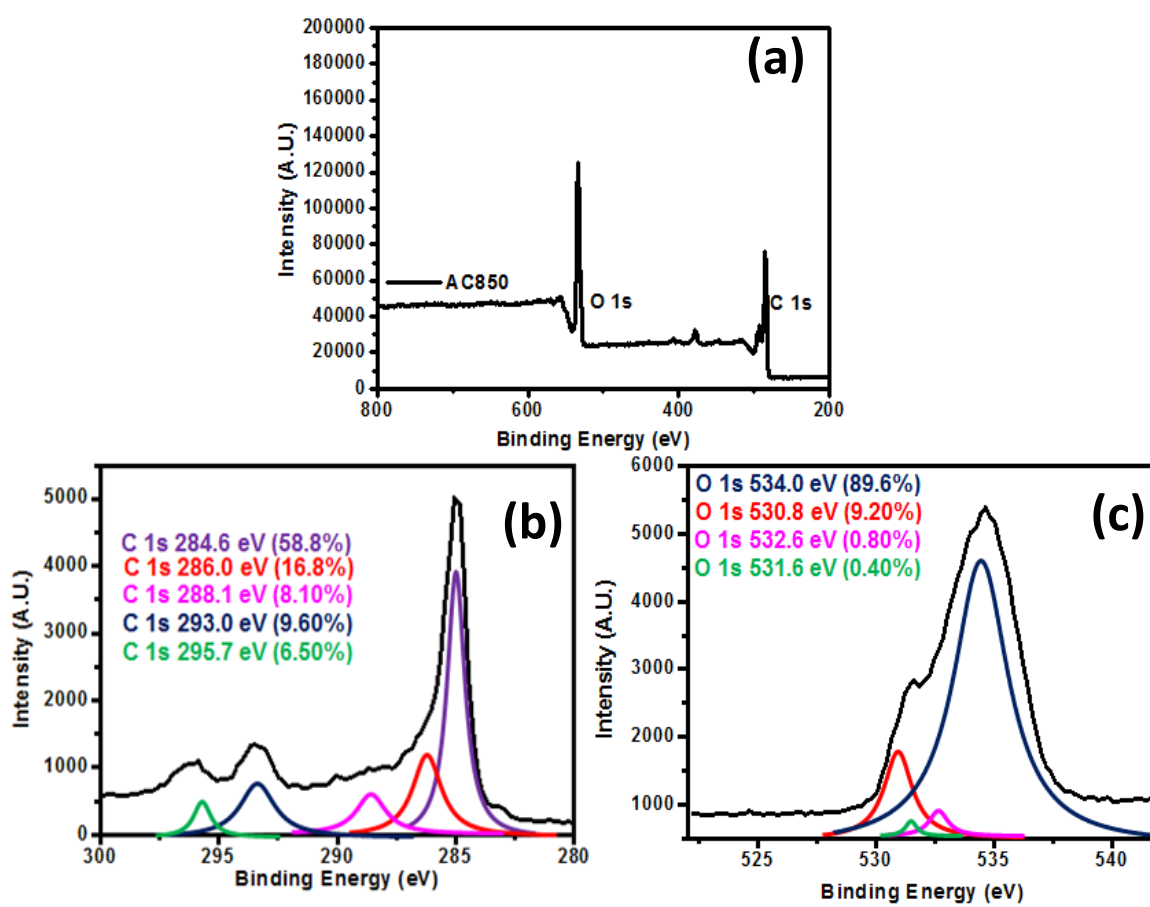
Figure 2
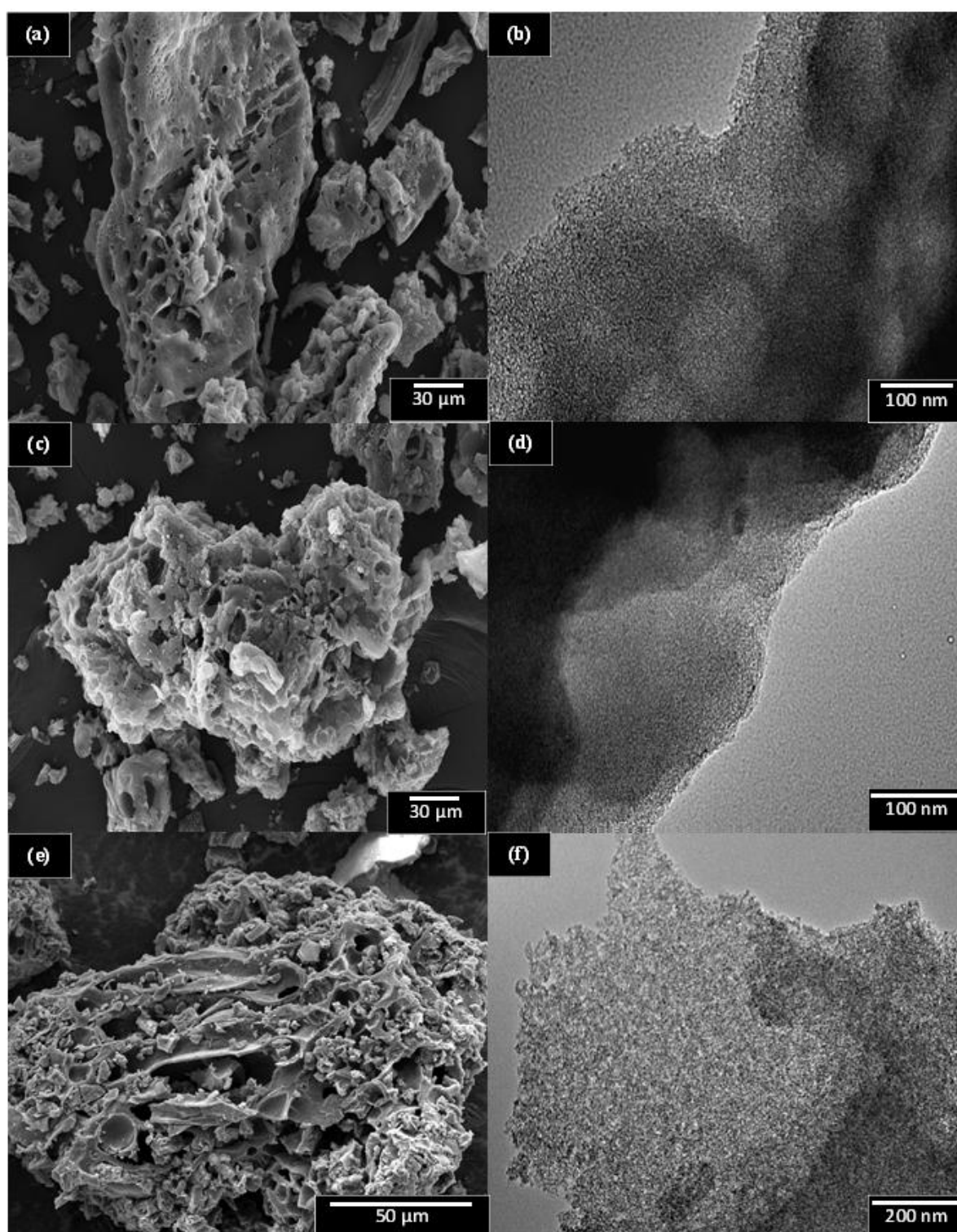
Figure 3
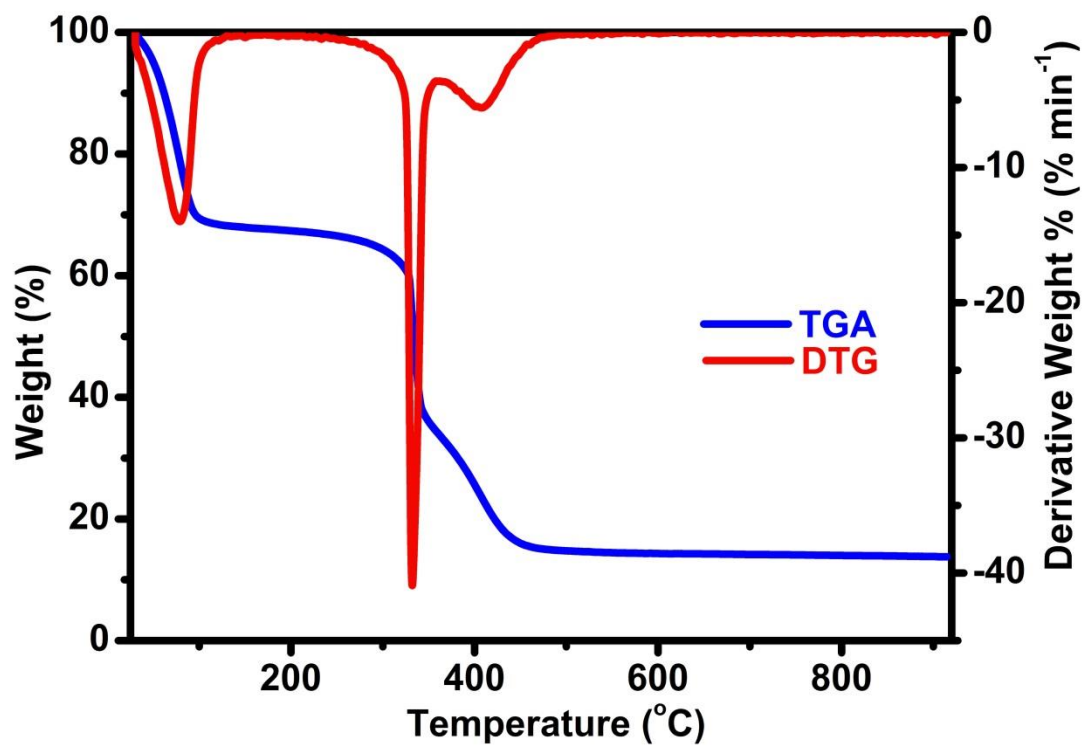
Figure 4
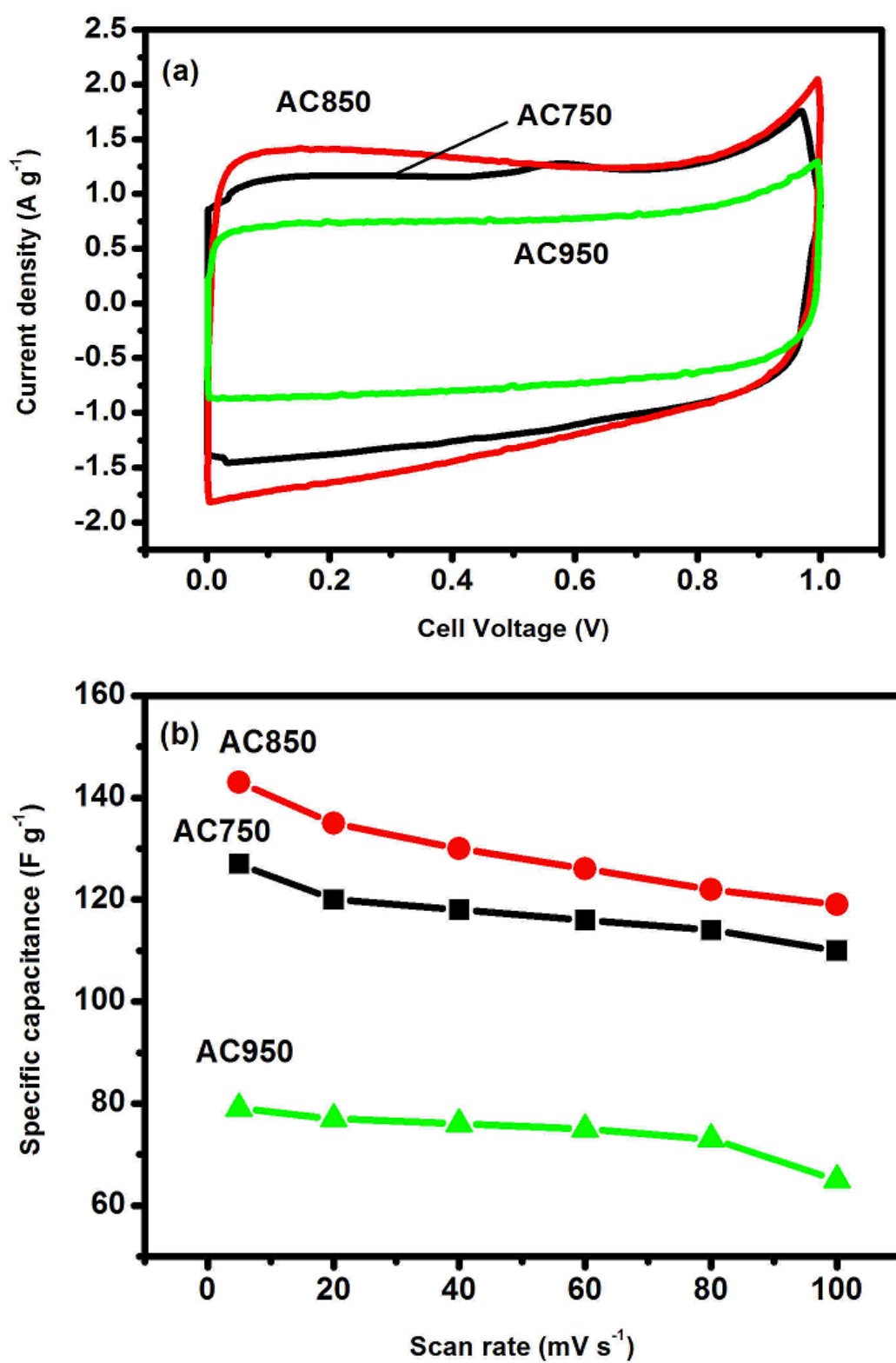
Figure 5
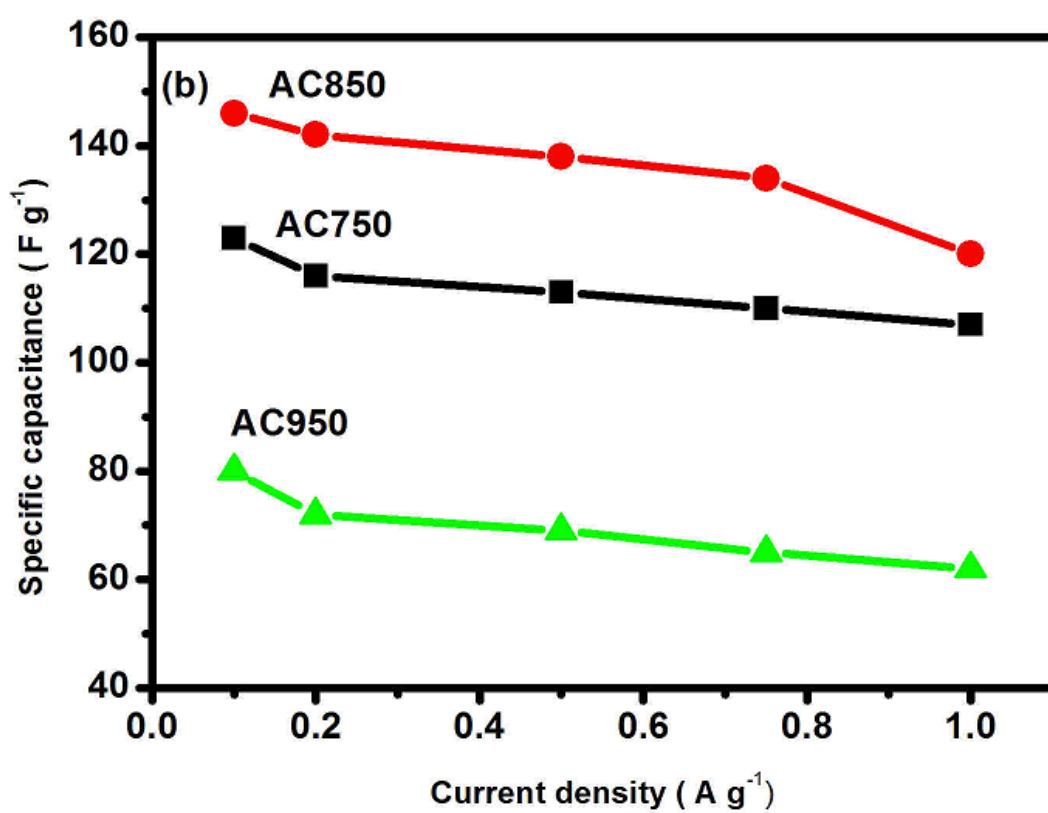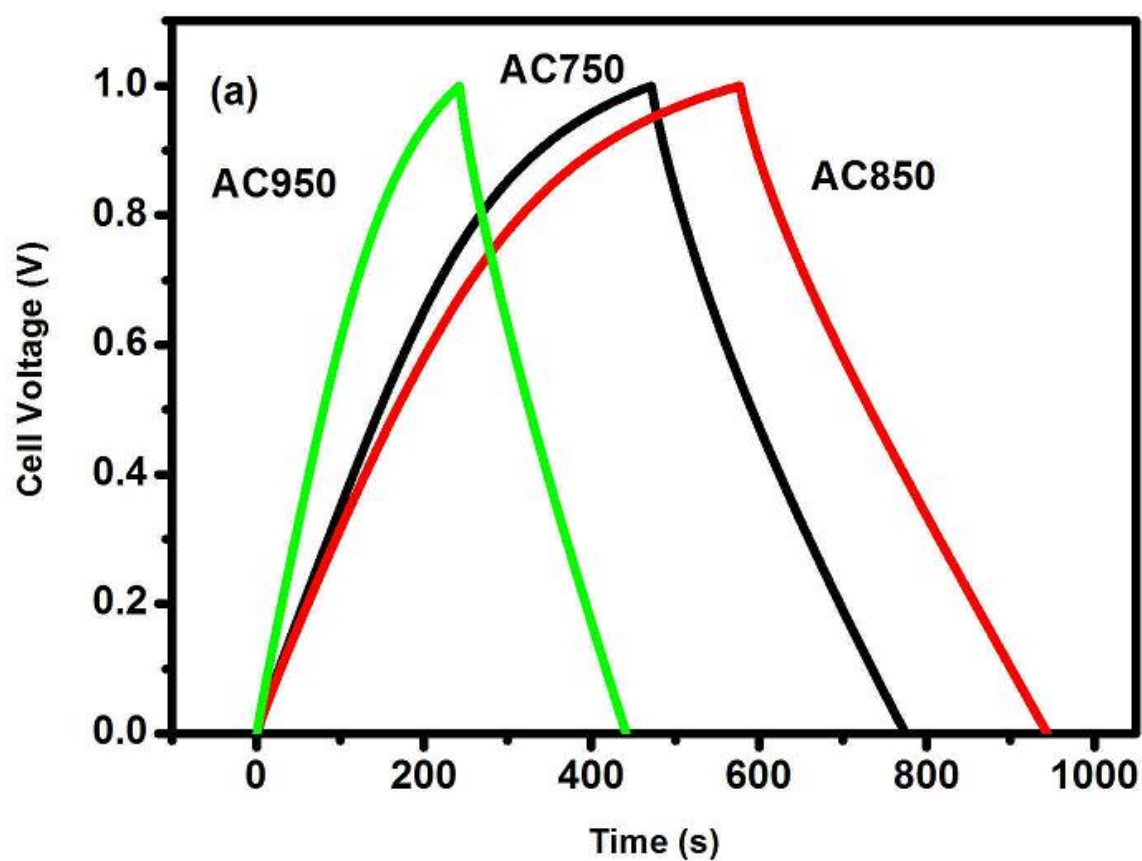
Figure 6
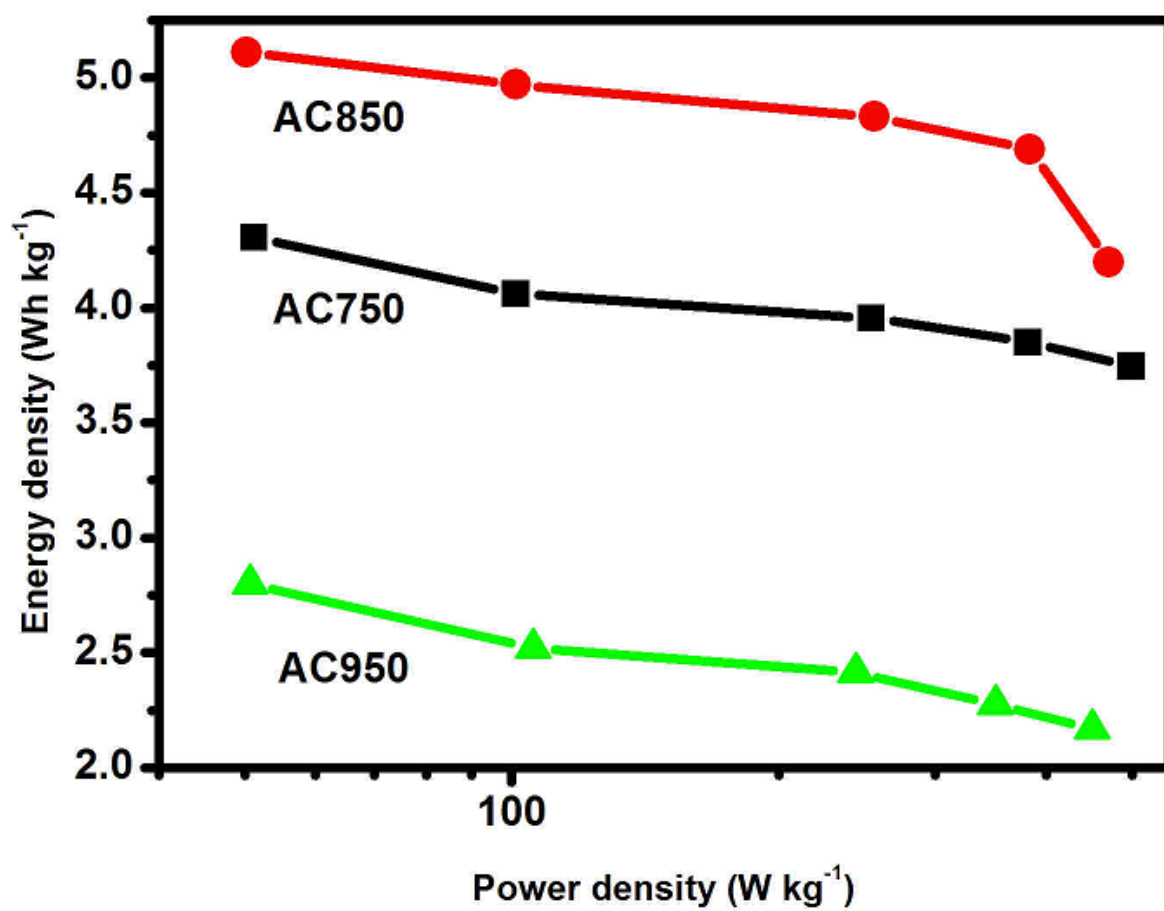
Figure 7
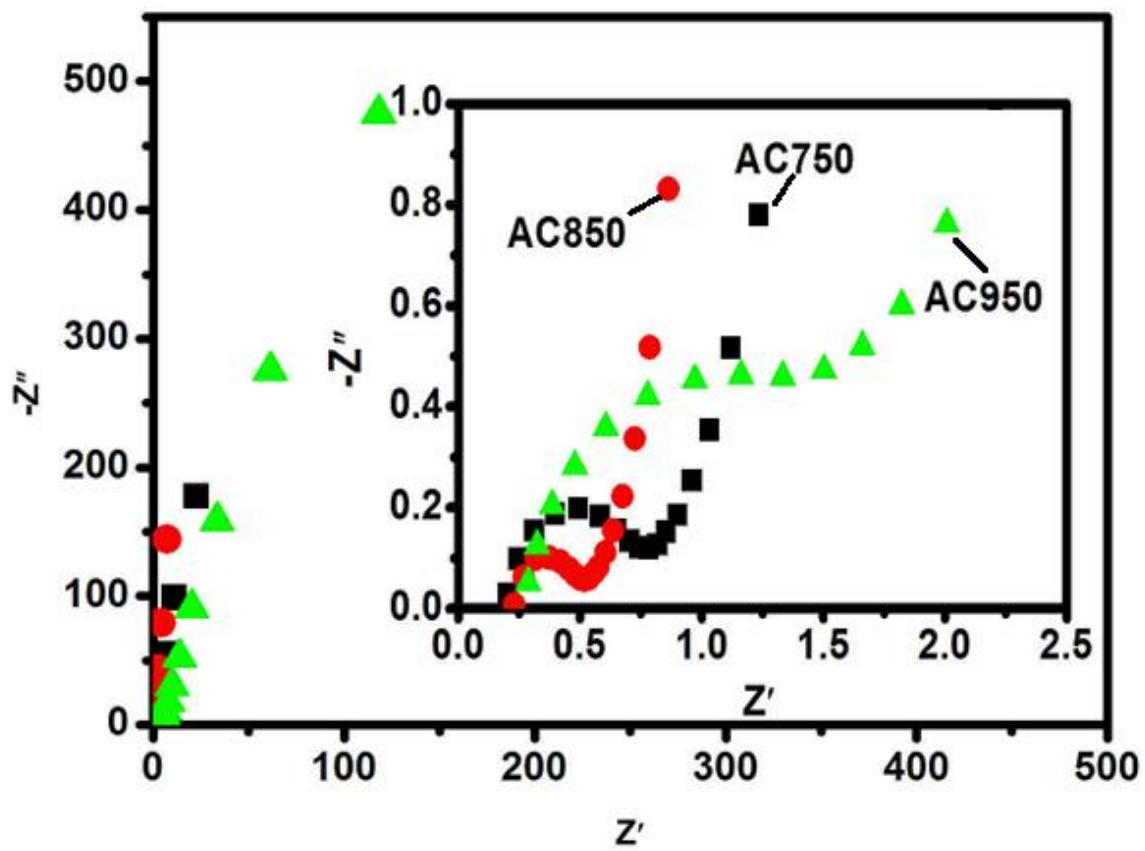
Figure 8
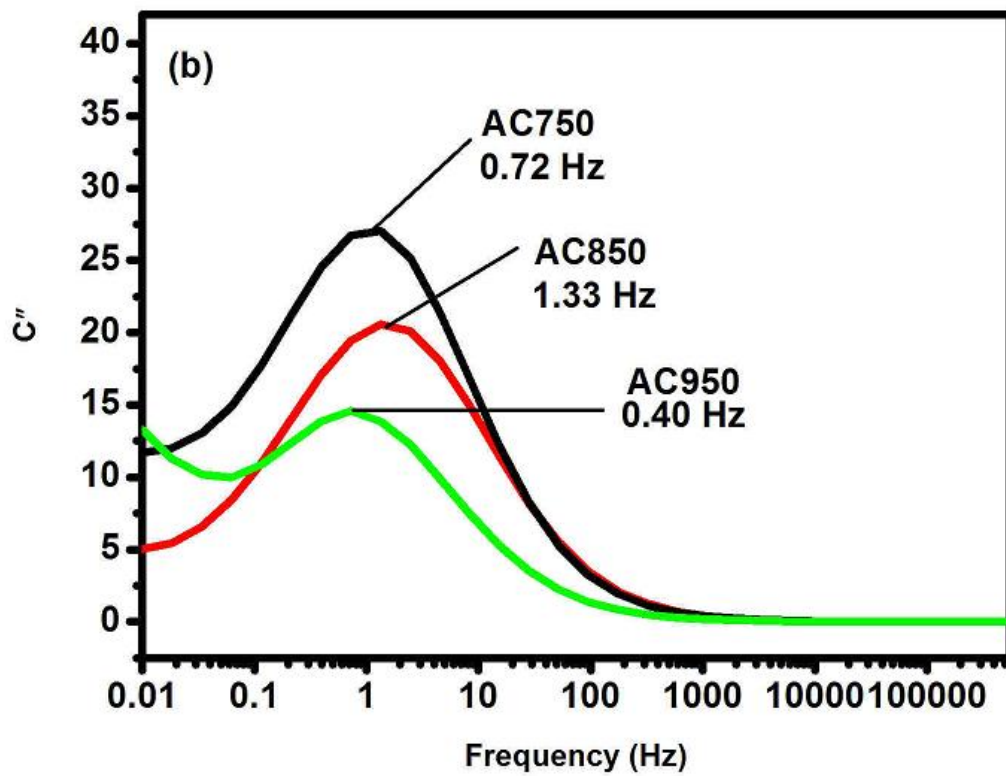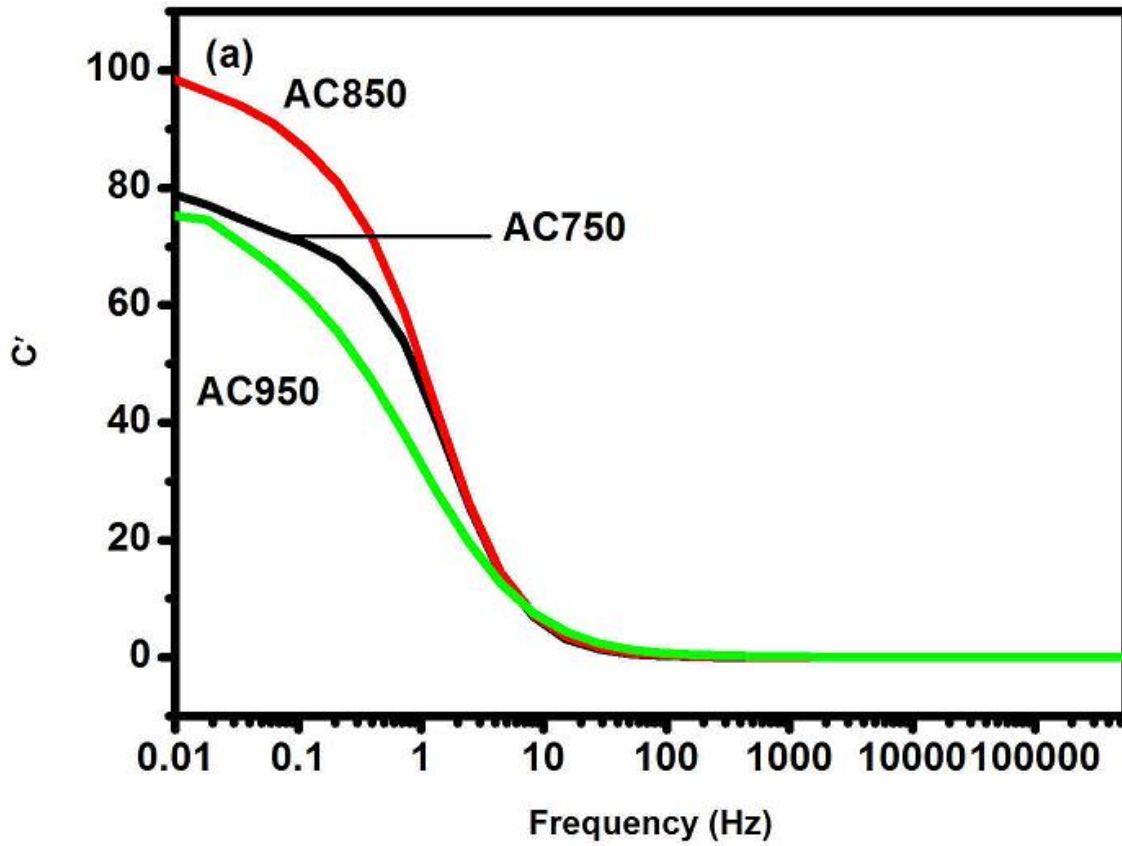
Figure 9
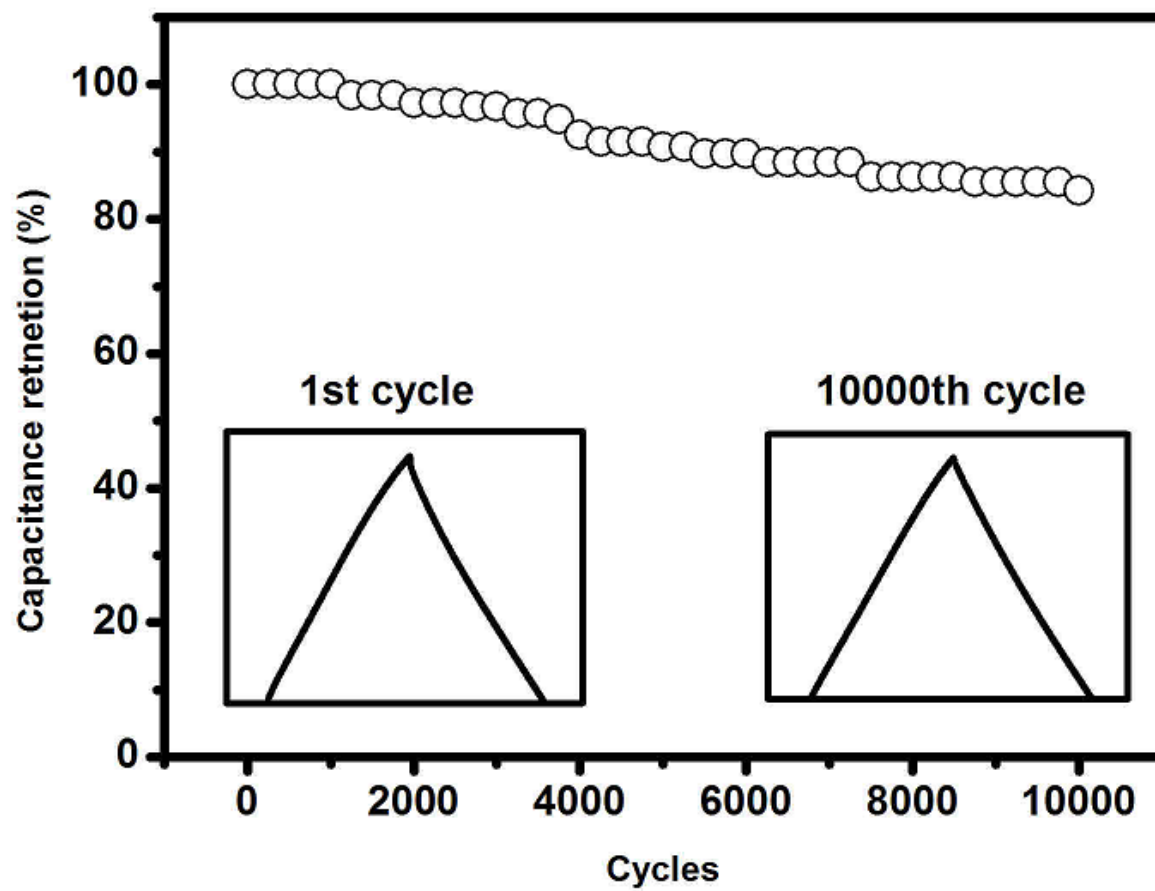
Figure 10

Scheme 1 The collapse of micropores and the generation of meso/macropores upon increasing the activation temperature from 750 °C to 950 °C.

Formation of porous structures in the AC samples upon activation with KOH from the relatively non-porous rice husk charcoal (RHC)
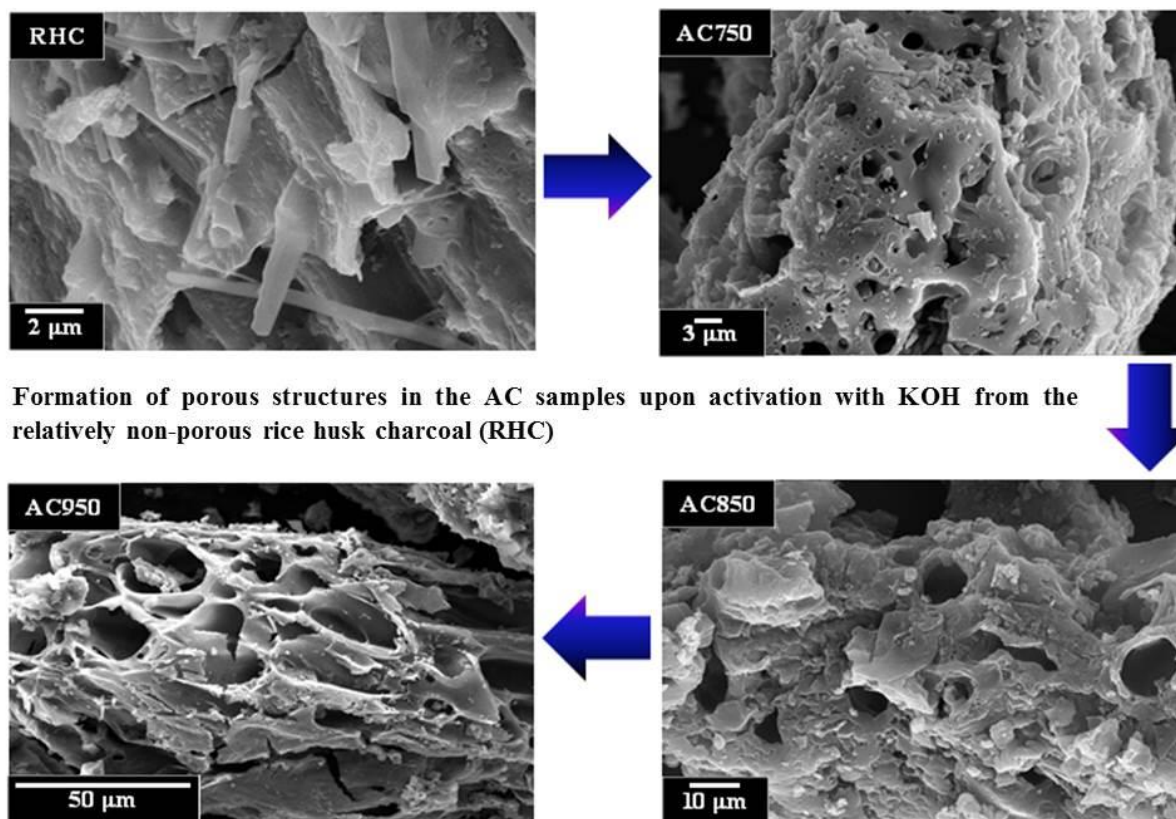
Pore widening upon increasing the activation temperature from 750 °C to 950 °C. The micropores tend to collapse upon high activation temperatures forming larger meso/macropores.

Scheme 2

Tables

Table 1 Textural and Raman spectral values of the AC samples used in the present study.

Sample	S_{BET} $(m^2\,g^{-1})$	V_{pore} (Total) $(cm^3\,g^{-1})$	V_{pore} (micro) $(cm^3\,g^{-1})$	V_{pore} (meso) (cm^3g^{-1})	t-plot micropore area (m^2g^{-1})	I_D/I_G (R value)	L_a (nm)	FWHM (cm^{-1})	
								G Band	D Band
AC750	2121	1.022	0.589	0.243	1426	1.003	4.387	117.2	295.3
AC850	2696	1.496	0.274	0.691	486	1.072	4.104	110.3	222.2
AC950	1592	1.293	0.052	1.056	-	0.935	4.706	54.7	90.0

Table 2 Elemental analyses of the AC samples used in the present study.

Samples	Elements (%)			
	C	O	Si	K
AC750	79.36 (83.63)	11.80	1.88	6.96
AC850	91.09 (84.02)	7.06	0.26	1.59
AC950	72.23 (79.86)	25.98	0.23	1.56

* Results in parentheses were obtained from TC analysis

Table 3 Comparison of AC derived from various biomass precursors.

Biomass precursor	Activation method	S_{BET} $(m^2\,g^{-1})$	C_{sp} $(F\,g^{-1})$	Energy density $(W\,h\,Kg^{-1})$	Electrolyte	Ref.
Rice husk	KOH	2696	147	5.11	6 M KOH	This work
Banana fiber	$ZnCl_2$	686	74	-	1 M Na_2SO_4	[49]
Pistachio shell	KOH	1009	125	-	1 M HNO_3	[50]
Firwood	Steam	1130	142	-	1 M HNO_3	[51]
Oil palm empty fruit bunch	KOH + CO_2	1704	149	4.3	1 M H_2SO_4	[52]
Rubber wood saw dust	CO_2	912	138	-	1 M H_2SO_4	[53]
Oil palm kernel shell	Steam	727	123	-	1 M KOH	[54]
Cotton stalk	H_3PO_4	1481	114	-	1 M $TEABF_4$	[55]
Rice straw	H_3PO_4	396	112	-	1 M H_2SO_4	[56]
Rice husk	H_3PO_4	1493	112	15.5	1 M Na_2SO_4	[57]
Rice husk	CO_2	1500	19	-	1 M $TEABF_4$	[21]
Beer lees	KOH	3560	188	-	0.1 M H_2SO_4	[58]
Seaweeds	-	1300	264	19.5	1 M H_2SO_4	[59]
Wood saw dust	KOH	2960	236	-	1 M $TEABF_4$	[60]
Scrap waste tire	H_3PO_4	510	93	-	6 M KOH	[61]
Natural wood	KOH	2925	200	-	6 M KOH	[62]
Recycled waste paper	KOH	180	180	-	6 M KOH	[63]